remote sensing

MDPI

Article

Seasonal and Spatial Characteristics of Urban Heat Islands (UHIs) in Northern West Siberian Cities

Victoria Miles * and Igor Esau

Nansen Environmental and Remote Sensing Center/Bjerknes Centre for Climate Research, Thormøhlensgt 47, 5006 Bergen, Norway; igor.ezau@nersc.no

* Correspondence: victoria.miles@nersc.no; Tel.: +47-97-088-029

Received: 28 July 2017; Accepted: 18 September 2017; Published: 27 September 2017

Abstract: Anthropogenic heat and modified landscapes raise air and surface temperatures in urbanized areas around the globe. This phenomenon is widely known as an urban heat island (UHI). Previous UHI studies, and specifically those based on remote sensing data, have not included cities north of 60°N. A few in situ studies have indicated that even relatively small cities in high latitudes may exhibit significantly amplified UHIs. The UHI characteristics and factors controlling its intensity in high latitudes remain largely unknown. This study attempts to close this knowledge gap for 28 cities in northern West Siberia (NWS). NWS cities are convenient for urban intercomparison studies as they have relatively similar cold continental climates, and flat, rather homogeneous landscapes. We investigated the UHI in NWS cities using the moderate-resolution imaging spectroradiometer (MODIS) MOD 11A2 land surface temperature (LST) product in 8-day composites. The analysis reveals that all 28 NWS cities exhibit a persistent UHI in summer and winter. The LST analysis found differences in summer and winter regarding the UHI effect, and supports the hypothesis of seasonal differences in the causes of UHI formation. Correlation analysis found the strongest relationships between the UHI and population (log P). Regression models using log P alone could explain 65–67% of the variability of UHIs in the region. Additional explanatory power—at least in summer—is provided by the surrounding background temperatures, which themselves are strongly correlated with latitude. The performed regression analysis thus confirms the important role of the surrounding temperature in explaining spatial–temporal variation of UHI intensity. These findings suggest a climatological basis for these phenomena and, given the importance of climatic warming, an aspect that deserves future study.

Keywords: urban heat island; land surface temperature; land cover; remote sensing; MODIS; Siberia; Arctic

1. Introduction

Urbanization in the Arctic and sub-Arctic is an increasingly important factor for the anthropogenic influence on the local and regional climate and ecosystems. One of the most evident and widely documented climatological effects associated with urbanization is the urban heat island (UHI) effect, for which urban and suburban areas are warmer than rural areas [1,2]. Urban areas alter the weather and climate, and feedbacks influence human health and energy consumption; these two aspects alone are enough to motivate interest in UHI studies. UHIs affect the climate of cities [3], shift plant phenology [4] and develop habitats for introduced or invasive species of plants and animals [5]. With rising global warming, the intensity of the UHI is also likely to increase, and its effects will become more significant in the future [6].

Literature has revealed that the UHI effect increases with latitude [7]. There is, however, a significant knowledge gap, as all but a few of the studied cities have been located below 60°N latitude. There are only a few in situ studies of the UHI effect for cities and towns above 60°N [8,9].

Although the high-latitude UHI has received relatively little attention in literature, there is a growing demand to identify the relevant physical and ecological processes.

Increasing UHI temperatures induce more significant impact in high latitudes, threatening the infrastructure, building and road stability [10]. Shiklomanov et al. (2016) [11] have already found a weakening of the soil bearing capacity and an increasing vulnerability of urban infrastructure to increasing surface temperatures in the cold climate regions. Other authors have associated shifting phenological phases [12] and the advance of alternative ecosystems [13] to higher urban temperatures.

The question regarding effective drivers for the UHI in high latitudes remains unresolved. UHIs in low latitudes and mid-latitudes are typically driven by a reduction in evaporative cooling over urban landscapes [3]. A number of studies suggest that anthropogenic heating [1] as well as CO_2 and pollutant emissions [14,15] additionally increase the urban–rural temperature difference. There are also statistical linkages between the UHI intensity and various descriptive indicators of cities, such as the urban area size and its density and population. Imhoff et al. (2010) [16] suggest that the effect is more or less pronounced depending on the type of landscape. The intensity of the UHI depends on the ecosystem it replaced. In the boreal forest environment, forest cleanings are found to have a local cooling effect [17], thus damping the UHI intensity. UHIs also depend on the regional climate [3], forming a rather distinct annual cycle in the northern climate zones [18]. At the same time, within the same ecological background, larger cities have larger heat islands in terms of both magnitude and area [14,18].

The UHI can be identified by comparing air temperature observations from a meteorological station network or from special observational campaigns [9,19]. Urban observational networks are, however, sparse and are often non-representative in complex anthropogenic landscapes. Moreover, not every city has pairs of rural and urban weather stations, and it is difficult to rely on in situ data alone to obtain information about the UHI. Therefore, urban climatologists are increasingly referring to the remotely sensed land surface temperature (LST) as a convenient and accessible means to characterize UHIs (or surface urban heat islands (SUHIs) [20]). Because no commonly accepted terminology is in use, we refer in this study to UHI when discussing general effects of the urban temperature anomaly, whereas SUHI is used when LST data and features are specifically addressed. This separation was proposed by Vogt (2004) [21] and was followed by Huang et al. (2017) [22].

The use of satellite remote-sensing data, such as the LST data from the moderate-resolution imaging spectroradiometer (MODIS), makes it possible to study the UHI of a large number of cities. The MODIS is particularly useful for LST data because of its global coverage, radiometric resolution and dynamic range for a variety of land-cover (LC) types. It has high calibration accuracy in multiple thermal infrared bands designed for retrievals of LST and atmospheric properties [23]. Despite some noted difficulties and inaccuracies [24,25], the LST data retrieved by the MODIS sensors aboard the Terra (EOS AM) and Aqua (EOS PM) NASA satellites are widely used for UHI studies [16,26,27].

Here, we use MODIS LST data to test the UHI effect north of 60°N, focused on northern West Siberia (hereafter NWS). There are strong physical reasons to expect that the cold continental climate in the NWS region could exacerbate the UHI trapping the additional heat in a shallow planetary boundary layer of the persistently stably stratified lower atmosphere [28,29]. These factors make this region an ideal testbed to study the intensity, magnitude, and spatial and temporal variability of the UHI effect in high latitudes, here for the first time for a large number of cases spanning an extensive area.

2. Materials and Methods

2.1. Study Area

NWS is defined as the territory east of the Ural Mountains and west of the Yenisei River (Figure 1). On a political map, the study area includes two administrative districts (okrugs): Yamalo-Nenets

Autonomous Okrug and Khanty-Mansi Autonomous Okrug. The largest cities are Surgut (population of ~332,000), Nizhnevartovsk (266,000), Nefteyugansk (126,000) and Noyabrsk (107,000).

Recent exploration and exploitation of oil and gas reserves in the region has led to rapid industrialization and urban development, and more than 90% of Russia's natural gas is produced there. The region also accounts for 63% of Russia's oil production. Nearly 1.8 million people live in NWS and 85% of the population is concentrated in the cities. We study 28 cities varying in population and area but found on the background of relatively homogeneous large-scale LC. The NWS landscape is nearly flat, and more than 50% of the area lies below 100 meters above sea level. NWS is a bogged region; in some parts, mires cover up to 70–80%. Forest covers only 36% of NWS.

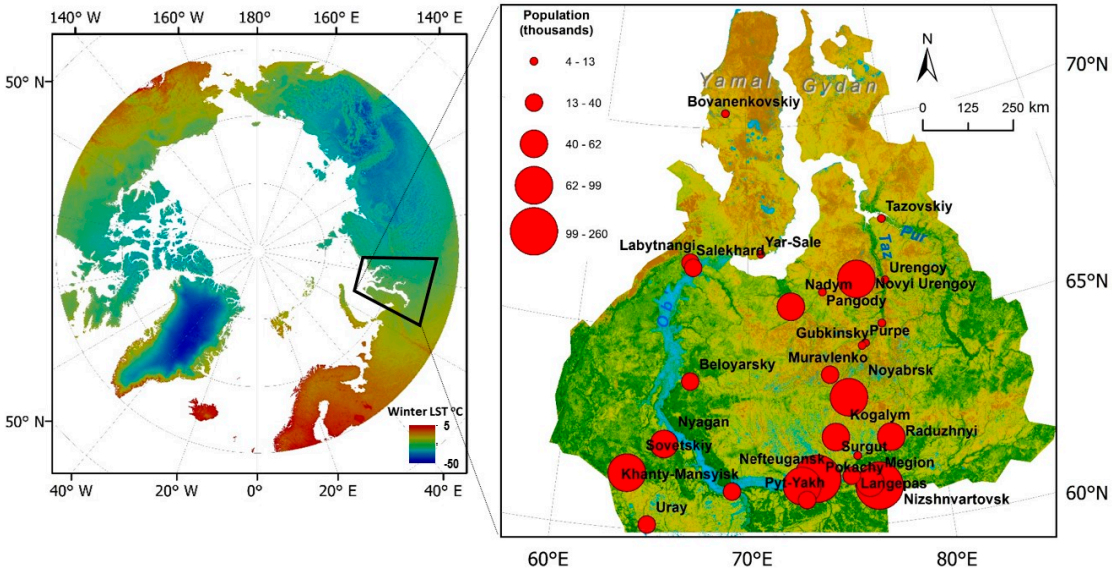


Figure 1. (**a**) Location of study area. Pan-Arctic 15-year (2000–2016) winter moderate-resolution imaging spectroradiometer land surface temperature (MODIS LST) composite. (**b**) Twenty-eight studied cities and relative city size. Background represents the 15-year (2000–2016) mean vegetation productivity (the annual normalized difference vegetation index (NDVI) max [13]).

The climate of the NWS region is continental and of the Dfc type (cold, fully humid climate with snow) according to the Koeppen–Geiger classification [30]. The mean winter surface temperature and amount of snow decrease in the northeastern direction, according to the Russian National Climate Atlas. The winters are cold, with stable snow cover from October through April (200 to 230 days per annum). The mean January temperatures are between −22 °C in Khanty-Mansiysk and –29°C in Tazovsky. The mean July temperatures are distributed more uniformly with a South–North temperature decrease from +17 °C (in the cities along the middle Ob River) to +14 °C (in the northernmost cities). The mean annual surface air temperatures are between −2 °C and −9 °C, that is, on average below the water freezing point. Permafrost however remains isolated, sporadic and discontinuous because of significant snow depth (about 150 cm by the end of the season), according to the International Permafrost Association (*https://ipa.arcticportal.org/*). Permafrost is a significant factor impacting the land temperature and surface LC only in the northernmost NWS cities [10]. Although the NWS climate is fully humid because of low temperatures and reduced evaporation, the cloud cover in the region is relatively moderate (60%) with a large number of clear-sky days (1600 h of annual sunshine), particularly in the winter season. The latter climatic feature makes this study representative and climatically robust.

2.2. Data and Methods

To identify thermal anomalies associated with urban areas, we used the Terra-MODIS LST data from 2001 to 2015. The LST and emissivity product, MOD11A2, of Terra-MODIS was used in the study. MOD11A2 is an 8-day LST product of averaging from 2 to 8 days of the clear-sky MOD11A1 daily product of Terra-MODIS, and it has 12 Science Data Set (SDS) layers [31]. A split-window algorithm is used for calculating LSTs. The day/night LST method retrieves the LST and band emissivity simultaneously from pairs of daytime and night-time MODIS data in seven Thermal Infrared (TIR) bands.

LST composites were downloaded from *http://reverb.echo.nasa.gov/*. The downloaded data were in HDF-EOS format and in the sinusoidal projection system. The data were re-projected from the sinusoidal projection to the Universal Transverse Mercator (UTM) zone 42°N projection system with the WGS84 datum, reformatted from HDF-EOS to GeoTIFF format and converted from °K to °C.

According to the product quality control flag, the data we used had an average LST error of $\leq$2 °C. The analysis was carried out for winter (DFJ) and summer (JJA) seasons. We processed day and night LST data. For Terra-MODIS, the satellite overpass times are approximately 10:30 and 22:30 local time.

Different studies comparing the MODIS LST with in situ observed and reanalysis gridded air surface temperatures report controversial conclusions and very fragmented mean temperature-difference maps. The MODIS LST from the Terra and Aqua platforms were compared with the air temperature from northern North American stations [32]. They showed that both the daytime and nighttime differences were in all cases smaller for Terra-MODIS LST. The mean difference (MODIS station) was found to be $\leq$2 °C for all stations. This finding is inconsistent with another study [33] for a selection of mid-latitude North American stations. The latter study found that the night-time Aqua-MODIS LST had smaller differences in surface air temperature than the Terra-MODIS LST. Comparing these results, as well as reports from other, less-representative studies (e.g., [25]), one has to be cautious about systematic urban biases in the MODIS LST data. This question is rather unclear in the present context because, as mentioned above, high-latitude cities generally have no in situ observational networks and no detailed UHI studies have been conducted there previously. For each city, we computed the annual mean LST per pixel by aggregating the available 8 day mean composite separately for winter and summer. The daytime and night-time UHIs were calculated separately. Both the seasonal and annual average daytime and night-time values were computed. The mean values were calculated on the basis of the 14 year time series. As a result, we produced annual and temporally averaged summer and winter LST maps for each city.

We define the UHI as the difference of urban and rural areas, ΔT. The magnitude of ΔT is insensitive to the number of urban–rural pixels [34]. Urban pixels were allocated by city polygon; the surrounding, non-urban land in a 2 km buffer was considered as rural. Rural pixels were classified as natural surfaces of different LC types. We excluded water because it can significantly influence the LST [18,34]. All pixels related to urban or artificial surfaces in the rural zone were also excluded. The resulting ΔT value represents the difference between the maximum temperature of the city cluster ($TUmax$) and the mean temperature of minimally developed land outside the city (Tr):

$$\Delta T = TUmax - Tr \quad (1)$$

To explore the drivers of surface UHI, we combined satellite observations of LST and LC. Climate Change Initiative (CCI) LC data (from the European Space Agency (ESA)) were used in this study. The CCI 300 m data are annual global LC time series from 1992 to 2015. This unique dataset was produced by the reprocessing and interpretation of five different satellite missions. The data were issued by the ESA CCI and are publicly available. In the current study, we use the data for 2015. The spatial resolution is 300 $\times$ 300 m. An example of a LC map around the city Nefteyugansk is shown in Figure 2a. Table 1 provides an overview of the LC classes that we found around the cities in NWS. The typology counts 18 classes.

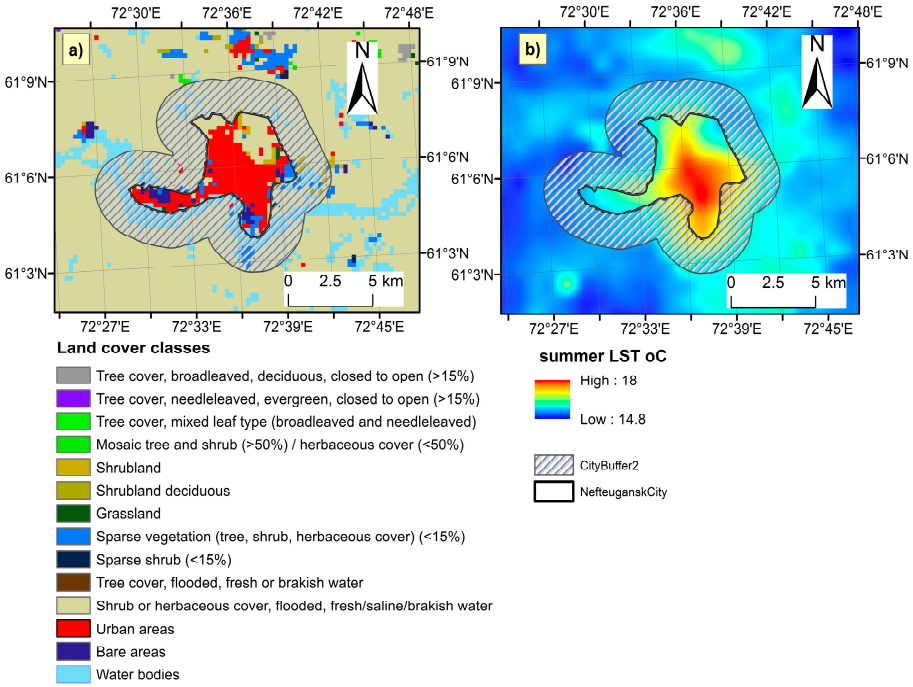


Figure 2. Example of Nefteyugansk City polygon and city cluster and a land surface temperature (LST) pattern. (**a**) Urban polygon and urban cluster identified by land cover Climate Change Initiative (LC CCI) and 2 km boundary buffer. (**b**) LST for the same area as in Figure 1a, on the basis of 15-year average moderate-resolution imaging spectroradiometer (MODIS) LST data. The urban cluster and the urban heat distribution are in agreement.

Table 1. Land cover class typology.

Value	Label
20	Mosaic cropland (50–70%)/vegetation (grassland/shrubland/forest; 20–50%)
30	Mosaic vegetation (grassland/shrubland/forest; 50–70%)/cropland (20–50%)
40	Closed to open (>15%) broad-leaved evergreen or semi-deciduous forest (>5 m)
50	Closed (>40%) broad-leaved deciduous forest (>5 m)
60	Open (15–40%) broad-leaved deciduous forest/woodland (>5 m)
70	Closed (>40%) needle-leaved evergreen forest (>5 m)
90	Open (15–40%) needle-leaved deciduous or evergreen forest (>5 m)
100	Closed to open (>15%) mixed broad-leaved and needle-leaved forest (>5 m)
110	Mosaic forest or shrubland (50–70%)/grassland (20–50%)
120	Mosaic grassland (50–70%)/forest or shrubland (20–50%)
130	Closed to open (>15%) (broad- or needle-leaved, evergreen or deciduous) shrubland (<5 m)
140	Closed to open (>15%) herbaceous vegetation (grassland, or lichens/mosses)
150	Sparse (<15%) vegetation
170	Closed (>40%) broad-leaved forest or shrubland permanently flooded
180	Closed to open (>15%) grassland or woody vegetation on regularly flooded or waterlogged soil water
190	Artificial surfaces and associated areas (urban areas >50%)
200	Bare areas
210	Water bodies

The city edge polygons were downloaded from the Russian Demographic Database (http://www.grid.unep.ch/russia/). Because administrative city boundaries differed from the true extents, each polygon was manually corrected using ArcGIS base maps. Further, we identified cities in the form of special clusters of urban LC. The city polygon was used to determine a 2 km buffer around urban clusters. The approach was partially adopted from that by Zhou et al. (2013) and Wang et al. (2016) [18,35]. All GIS and remote-sensing data were processed using ArcGIS 10.3 software. Figure 2 shows the city polygon and 2 km buffer polygon.

The degree of homogeneity or heterogeneity of the LC can be analyzed by measuring the number of different LC types in each city buffer and their relative abundance. The Shannon evenness index

(*SHEI*) [36] was used to evaluate landscape diversity, and takes into consideration both the number of different LC types and their relative abundance. The index is based on values within the range of 0–1; zero represents a landscape with no diversity (only one LC type) and a value of 1 represents the maximum diversity (featuring all types of LC in equal amounts):

$$SHEI = -\sum (Pi * \ln (Pi))/\ln(m) \quad (2)$$

where the relative abundance (proportion) of LC types is denoted by *Pi* and the different types of LC are denoted by *m*.

We analyzed the UHI intensity for all cities. In order to identify the factors underlying the observed UHIs, several plausibly related variables were considered. Relationships between the variables were investigated using correlation analysis and multiple ordinary least squares (OLS) regression, where we used summer ΔTs and winter ΔTw as the dependent variable and a number of independent or predictor variables: latitude $|\phi|$, Tr; city area (*S*); population (*P* and log*(P))* and *SHEI*. In addition, for summer, parameters such as vegetation greenness in and around the city approximated by the normalized difference vegetation index (NDVI) were also included in the statistical analysis. This study utilized MODIS NDVI 16 day composites with a 250 m spatial resolution (MOD13Q1) onboard the Earth Observing System-Terra platform satellite for the period 2000–2016. This study was based on the maximum summer NDVI, denoted as *NDVImax* [37,38]. The statistical significance for the correlation analysis was based on a non-directional (two-tailed) null hypothesis, except for the population (*P* and log*(P)*) and area of the cities, for which any significant correlation was assumed a priori to be positive. Statistical calculations were made using the SPSS statistical package.

3. Results

3.1. Urban Heat Island

On the basis of 15 years of MODIS LST data, the study confirms the prevalence of UHIs in the studied cities in both seasons, winter and summer (Figure 3). There are a few exceptions—for three cities in the north of the region (above 64°N latitude) for the summer season, the opposite UHI was found. Comparing daytime and night-time anomalies, the summer UHI of these three cities is greater during the night—the Yar-Sale night-time UHI effect even becomes positive. At the same time, all of the other cities show higher UHIs in daytime than in night-time.

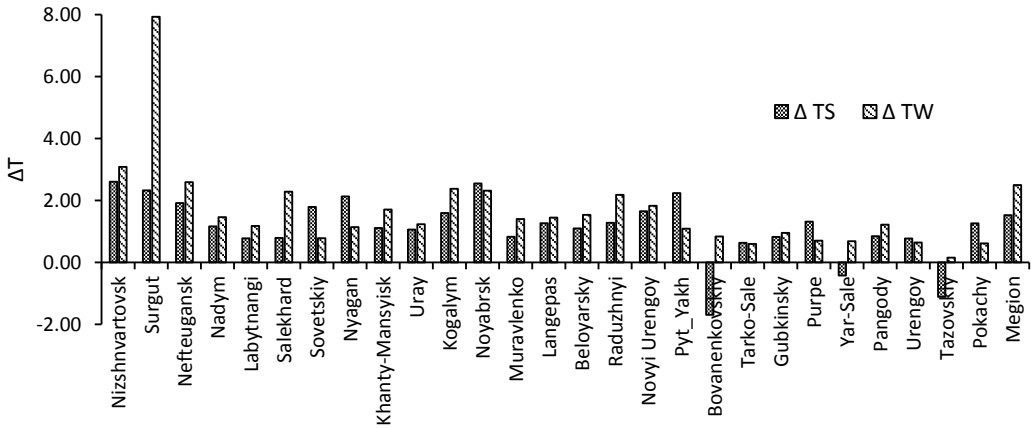


Figure 3. Winter (ΔTw) and summer (ΔTs) urban heat island (UHI) in 28 studies cities in northern West Siberia (NWS).

Every city has a winter UHI and in 60% of cases it is higher than the summer UHI. For winter, most of the cities have a larger night-time UHI than daytime UHI. For the special case of Surgut, the winter

UHIs are extreme, likely as a result of the location of the Surgut-1 and -2 thermal power stations (Figure 4), which are combined cycle gas-fired power stations. With an installed capacity of 5597 MW, Surgut-2 is the largest gas-fired power station in the world. Surgut-2 consumes approximately 10 billion cubic meters of natural gas annually. The pixel related to the Surgut power station and adjacent reservoir fed by the Ob River is clearly visible on the MODIS LST image (Figure 4). The water is used for cooling and has a surface water temperature significantly higher than that of the surrounding land for a major part of the year. The difference is particularly large in wintertime. The temperature footprint extends for several kilometers in all directions, sometimes reaching the Surgut airport at a distance of 4 km to the north. We are not aware of any detailed study of this heating footprint in either English or Russian literature.

Rural temperature (*Trw*) is also higher for Surgut than for neighboring cities, as Surgut is also the largest city of the area. A statistical analysis for winter was performed both using all cases and without the extreme case of Surgut.

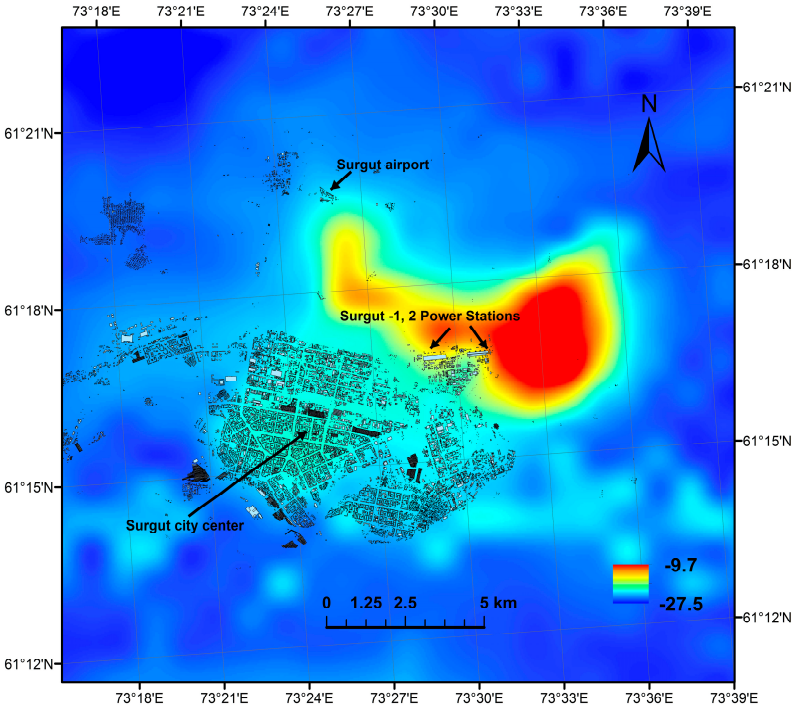


Figure 4. Example of the extreme case of Surgut. Surgut winter land surface temperature (LST). Black line contours denote the city building polygons. Numbers represent LST values in degrees Celsius.

3.2. Correlation and Regression Analysis

3.2.1. Correlation Analysis

A correlation analysis was performed in order to explore relationships that may explain spatial and seasonal differences in the UHIs of the study area. Table 2 shows Pearson's correlation coefficient (r) between ΔT and several of the studied variables, stratified by season (winter and summer). Both ΔTs and ΔTw show the strongest correlations (r of 0.81 and 0.82, respectively) with the city population (log P)—see Figure 5. The correlation between the UHI and city area is also strong and significant, because the city area and population are positively correlated with each other.

Further, the mean urban-to-rural temperature differences (ΔT) and rural background temperature (Tr) are negatively correlated with latitude $|\phi|$, suggesting that the UHI intensity depends, among other parameters, on the background temperature itself. The summer UHI (ΔTs) shows a decreasing

trend from low to high latitude (Figure 5a) and shows a strong correspondence with the surrounding temperature (*Trs*; Figure 6c).

Table 2. Pearson's correlation coefficients (r) for urban heat island intensity (ΔT) and other—rural temperature (Tr), Shannon evenness index ($SHEI$), logarithm of population ($\log(P)$) and area—for (a) summer and (b) winter. Bold underline indicates correlations significant at the 0.01 level and underline indicates correlations significant at the 0.05 level (N = 28 (summer); N = 27 (winter)).

(a) Summer					
	Trs	**ΔTs**	***SHEI***	**log(*P*)**	**Area (km^2)**
$\lvert\phi\rvert$	**–0.93**	**–0.77**	0.44	**–0.63**	–0.38
Trs		**0.73**	–0.44	**0.67**	0.40
ΔTs			–0.25	**0.81**	**0.50**
SHEI				–0.36	–0.30
log(*P*)					**0.61**
(b) Winter					
	Trw	**ΔTw**	***SHEI***	**log(*P*)**	**Area (km^2)**
$\lvert\phi\rvert$	**–0.63**	–0.39	0.47	**–0.62**	–0.36
Trw		0.15	–0.28	0.35	0.01
ΔTw			**–0.52**	**0.82**	**0.64**
SHEI				–0.45	–0.32
log(*P*)					**0.60**

Arguably, the strong negative correlation between the rural background temperature (Tr) and latitude $\lvert\phi\rvert$ reflects the mean latitudinal climatic temperature gradient in NWS (Figure 5a). The positive dependence in summertime between the mean urban-to-rural temperature differences (ΔT) and Tr clearly identifies the large role of the incoming solar radiation in the UHI intensity (Figure 6c). Indeed, if the anthropogenic heat release (heat pollution) were dominant, then the correlation between Trs and ΔTs would not be so significant; it is 0.73 in our data. This is a non-trivial dependence, as the NWS cities have significantly higher summer albedo than the surrounding landscapes (boreal forest and shrubland). This larger UHI suggests that surface moisture, or more precisely, the Bowen ratio [39], plays a significant role. The urban runoff from impervious surfaces and water penetration into sandy soils make the surface itself significantly warmer and drier than the vegetated LC patches.

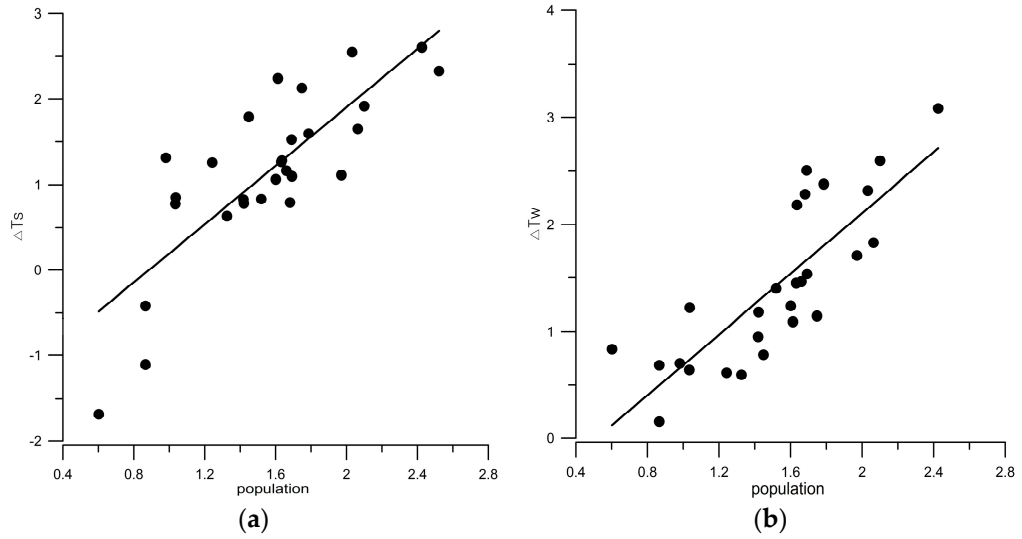


Figure 5. Relationship between urban heat island (UHI) intensity and logarithm of population (log P) in (**a**) summer and (**b**) winter. The least-squares best-fit line is indicated. Winter is shown excluding the outlier case.

The UHI (ΔT) shows no significant correlation with the land surface diversity (*SHEI*)—see Table 2—however, the summer mean LST (*Trs*) does have a significant, moderately negative correlation with *SHEI* ($r = 0.44$). Urban greenness may potentially play a significant role in the UHI formation. Here, the greenness was defined as the absolute values of the mean NDVI within the city limits (*NDVIc*) and as the absolute values of the mean NDVI around the city (*NDVIr*). Additionally, we considered how changes in vegetation in and around the city may influence the UHI. No significant relationships between ΔT and *NDVIc* and *NDVIr* were found.

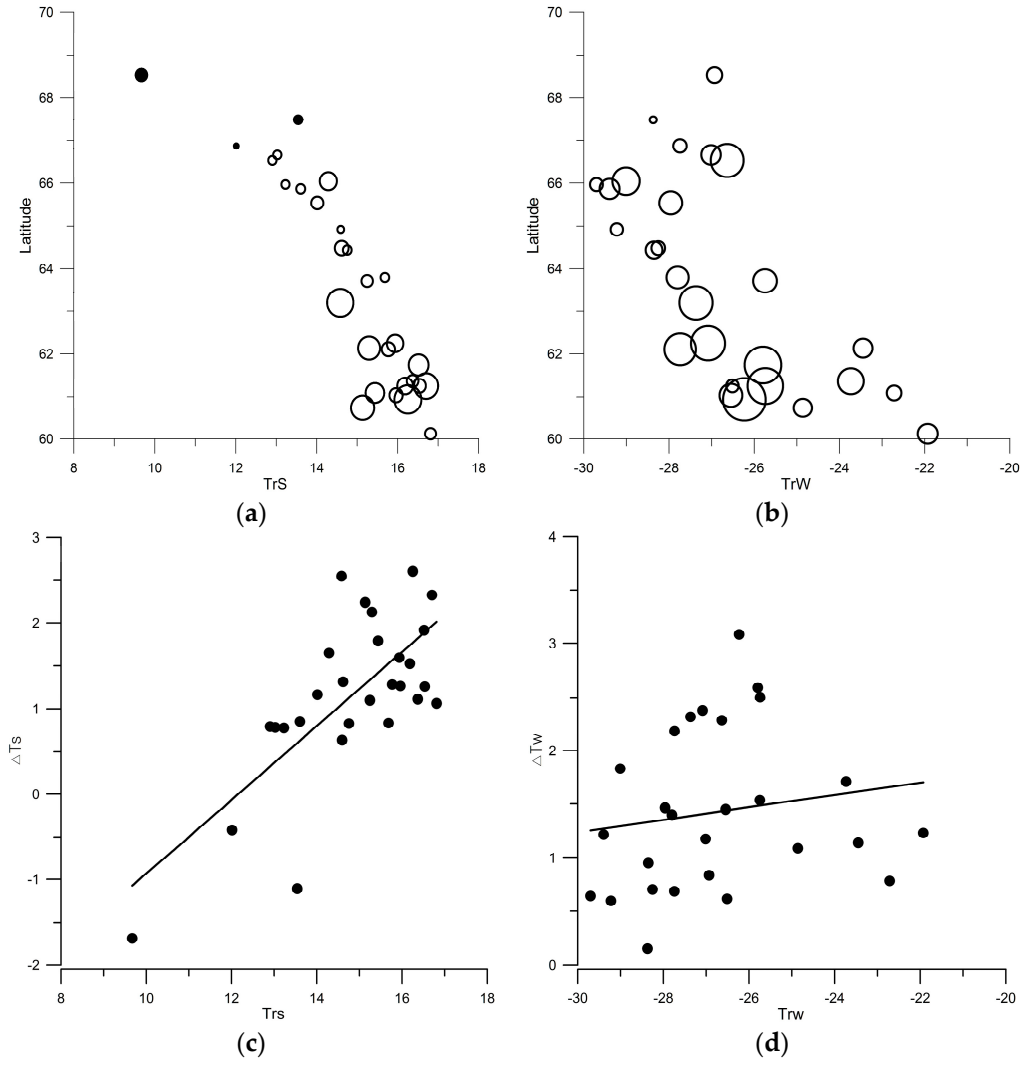


Figure 6. Dependence of urban heat island (UHI) intensity (ΔT) on latitude (**a**,**b**), and mean surrounding temperature (**c**,**d**) in summer and winter, respectively. The magnitude of UHI intensity is shown by circle size in (**a**,**b**); filled symbol indicates a negative UHI. *Trw* is shown excluding the outlier case.

3.2.2. Regression Analysis

The presence of several variables that are strongly and significantly correlated with ΔT warrants further analysis using regression methods, here using the stepwise method of variable selection in the framework of multiple regression modeling.

For summer, the initial model has one predictor variable ($\log(P)$; Equation (3)):

$$\Delta Ts = 1.71 \log P - 1.51 \quad (3)$$

The initial regression model has a coefficient of determination $R^2 = 0.65$, meaning that 65% of the variability in ΔTs can be "explained" or accounted for by the difference in population alone. Further selection of an additional predictor variable (*Trs*; Equation (4)) increases the R^2 value to 0.71:

$$\Delta Ts = 1.23 \log P + 0.20 Trs - 3.73 \quad (4)$$

For winter, the initial model (excluding the outlier Surgut) has one predictor variable (log*(P)*; Equation (5)):

$$\Delta Tw = 1.42 \log P - 0.73 \quad (5)$$

The simple regression model has a coefficient of determination $R^2 = 0.67$, which could not be increased by adding additional predictor variables within the constraining criteria of the multiple regression procedures.

4. Discussion

Most of the UHI intensity studies are limited to the 60°N latitude. In this study, we use remote sensing data from the MODIS platform to assess the UHIs and to define the most influential factor on UHI formation and intensity for the cities in NWS, which lies between 60°N and 70°N latitude.

We moved from an analysis of fragmented cases to an investigation of 28 NWS cities. A strong UHI is found in both summer and winter seasons. The mean UHI intensity is greater in the winter season. However, the expected dependence between the mean background temperature and winter UHI was not found. The anthropogenic heating does not overcompensate for the temperature drop, suggesting that the heat generation and distribution standards are sufficiently robust to account for the regional climate conditions. At the same time, the large UHI intensity and footprint area, as well as its strong dependence on the population, clearly identify that the standards do not account for the UHI. Urban temperature corrections for the heat distributing units could decrease the observed overheating with a considerable economic effect when accounting for more than 250 heating days per annum in the NWS.

The cold continental climates are characterized by prolonged periods of stable atmospheric stratification, when damped vertical turbulent mixing effectively traps the surface temperature anomalies in the lowermost air layers [26,27]. This trapping favors better agreement between the LST and the surface air temperature, as we have seen in the MODIS data discussion (Section 2). In such circumstances, the dominant urban development paradigm directed towards compact urban planning with a predominance of medium- and high-rise apartment blocks works for UHI intensification with all the noted detrimental consequences to the urban infrastructure. Norilsk is a clear example of the challenge [11]. This study shows that the UHI intensity is high and seasonally persistent in the NWS cities. Moreover, the urban green space intended to alleviate the UHI will likely result in the opposite effect. The boreal vegetation, particularly the dark coniferous trees and shrubs, has a warming rather than a cooling effect [17]. At the same time, the UHI may help to improve the city comfort and create an even deeper sense of place for the urban dwellers, supporting more diverse urban vegetation (see the review on the matter in [38]).

The leading UHI driver switches from anthropogenic to direct solar heating during the long summer days in northern latitudes. The short summer nights do not have analogs at other latitudes, and therefore the night-time UHI variability cannot be studied in other regions. The strong dependence of the summer UHI on the background temperature confirms the strong climatic basis for summer UHI formation. Zhou et al. (2013) [18] discovered increasing UHI intensities with an increasing boundary temperature for some cities in Europe. Synergistic interactions between UHIs and the warming climate are also evident (i.e., the magnitude of the urban–rural temperature difference is also increased when the background temperature increases) [40–42].

For three cities located in the tundra zone in the north of our study region (above 64°N latitude) for the summer season, an opposite UHI was found. Perhaps surprisingly, it is reminiscent of an

oasis effect [19] that typically exists in arid areas. Here, the towns have been built more recently and generally implement better construction standards. This reduces the UHI, making the higher albedo factor dominant. The background tundra vegetation (mostly lichens and dwarf shrubs) warms at greater rates as a result of a lower albedo than the urban area built on a sandy base and that has a very low amount of vegetation (high albedo).

There is no apparent relationship between UHI intensity and vegetation greenness in or around the cities. The general vegetation trend for NWS is an increase ("greening") in tundra and a decrease ("browning") in the boreal forest zone [13,42]. However, at the same time, it has been observed that there is an accelerated increase of the NDVI in the urban areas located in the taiga "browning" zone, and in contrast, a decreased NDVI in the tundra "greening" zone [37]. We did not establish a direct connection with vegetation greenness; however, there is some correlation between the UHI intensity and vegetation change in and around the city. The forest has warming effects in northern latitudes [17]; thus we can assume that an increase/decrease in the city vegetation can also have an effect on the UHI intensity and can cause an UHI increase in the southern part of the area and an UHI decrease in the northern part.

We did not find a significant correlation between the UHI and the land surface diversity (SHEI). This result, however, should not be misinterpreted. On the one hand, the largest surface difference was that between the urban and natural LC, although within each of these classes, the surface had relatively similar thermal properties. On the other hand, it is known that the impact of the surface heterogeneity scales is strongly non-linear and non-monotonic [43,44]. In most cases, it could be further moderated by the differences in the evapotranspiration [45]. Thus, it cannot be expected that the essentially linear statistical analysis, non-discriminative to the spatial scales, would reveal any UHI–SHEI dependences. The primary variables show that the summer mean LST has a significant negative correlation with the SHEI. This is an indicator that higher diversity or heterogeneity of LC around the city means that more heat is absorbed and possibly causes a cooling effect. Changes in vegetation and landscape diversity are plausible controlling factors of UHI intensity in high latitudes. More detailed studies of these effects are needed.

Earlier UHI studies (e.g., [1,46,47]) report a rather strong dependence between ΔT and the size of the urban population. The implication was that smaller cities should not exhibit considerable temperature anomalies compared to the regional climate. Later, using other UHI results, the dependences were found to be weaker and were even re-considered to be insignificant [48]. The dependence between ΔT and log P is the strongest statistical regression factor in NWS. However, its slope is more in line with results of recent studies [47] than with the earlier mega-city analysis.

There are some uncertainties and errors that could arise in our inferential study. Complex topography and LC are two influential factors on the LST [48]. The relationship between the LST and the influential factors varies with the seasons during the year, having either a warming or cooling effect on the Tr value. In NWS, the background surface heterogeneity around the urban areas is small-scale (much less than for the city areas), as has been objectively shown using Moran's I index [13]. In this region, the population is highly concentrated in a few compact and spatially well-separated urban centers. There are virtually no agricultural fields or smaller settlements between these centers. We studied 28 cities with strongly modified land-use/land-cover embedded at larger spatial scales into a relatively homogeneous natural environment.

The NWS landscape is nearly flat; therefore, topography would not be considered an influential factor in our case. However, despite the elimination of water and urban pixels because of their significant influence on the rural LST [35,49], we could still have an effect of these two LC classes on the results. Our study identifies the LC using 300 m ESA CCI data. According to the LC CCI accuracy assessment report, the LC data have uncertainties and limitations, mostly related to classification accuracy, and with an overall estimated accuracy of 71%. This indicates that, with such classification accuracy, the error in the eliminating of water and urban pixels is low.

The method used here and its implementation is to a large degree similar to those suggested in previous studies [18,35]. Using buffer zones to compute the urban–rural temperature difference has been widely practiced [48] and found to be consistent and robust for such an analysis. In our study, both the UHI and the rural background buffer could be unambiguously delimited in the NWS area. The study [3] of statistical connections between the UHI and the background climate in 65 U.S. cities used a method of pairing the pixels in the city centers with the rural buffer pixels. The author argued that this simpler delimitation is sufficient for region-wide studies of the UHI dependence for a selection of cities. The noted [50] study could be used as a strong background to support these simplest of choices. The latter authors used the objective Petit's and Rodionov's tests (individual point Student's *t*-tests) to determine the extent of the UHI in Bucharest. They reported that both methods are rather insensitive (i.e., statistically insignificant) to the urban–rural transition and the selection of the buffer zones. Thus, the conclusion, at least for the well-separated cities, was that the UHI intensity is rather insensitive to the chosen urban boundary delimitation method. In fact, we are working to extend our analysis of Siberian cities in order to include an analysis of the stability classes and typical synoptic situations in a way that is compatible with [51] but that uses the theoretical background presented in [52].

5. Conclusions

The main findings are the following:

(1). The analysis of the MODIS LST data products for 2000–2015 in this study revealed that all 28 NWS cities exhibit persistent UHIs. The UHI intensity is seasonally dependent. The seasonal mean is maximal in the winter UHI (1.6 °C). Northern settlements show a smaller UHI (average ΔTw of 1.4 °C and ΔTs of 0.3 °C) compared to the cities in the southern part of the area (average ΔTw of 1.9 °C and ΔTs of 1.1 °C).

(2). The analysis suggested different dominant driving factors for the UHI. In summertime, with its long days, the UHI intensity is mainly determined by surface albedo, reduced evaporation and the amount of incoming solar radiation. In wintertime, with its low temperatures and small amount of solar radiation, the UHI intensity is determined by anthropogenic heat pollution. A special case here is Surgut, which is an extreme example of the release of a huge amount of anthropogenic heat causing a large UHI in winter.

(3). Correlation and regression analyses found the strongest relationships between the UHI (ΔT) and population (log P). Regression models using log P alone can explain 65–67% of the variability of the UHI in the region. Additional explanatory power—at least in summer—is provided by the surrounding background temperatures, which themselves are strongly correlated with latitude. The performed regression analyses thus confirmed the important role of the surrounding temperature in explaining spatial–temporal variation in the UHI intensity. These findings suggest a climatological basis for these phenomena and, given the importance of climatic warming, this aspect deserves future study.

(4). The LC classification was used to distinguish between the urban and rural surfaces following the popular urban buffer approach. This study utilized the *SHEI* index to measure the surface heterogeneity. The *SHEI* index is only moderate (max value of 0.6) in NWS. The highest values were found in the northern part, where the land surface around the cities is less anthropogenically modified. The study did not reveal any statistically significant linear relations between ΔT and *SHEI*. However, a strong non-linearity of any such relations should be expected, as the response is likely to be amplified for certain scales of the surface heterogeneity.

(5). The study found an inverse UHI in the three northernmost cities. To discover the role of different land surface types in UHI formation, further exploration of land surface variables as a predictor for UHI intensity should be pursued in future studies.

Acknowledgments: This work was supported by the Belmont Forum and Norwegian Research Council project HIARC: Anthropogenic Heat Islands in the Arctic: Windows to the Future of the Regional Climates, by basic funding at the Nansen Center, by Ecosystems and Societies (No. 247468) and by the NordForsk project CRUCIAL. We thank the reviewers for their thorough reviews and highly appreciate the comments and suggestions, which significantly contributed to improving the quality of the publication. The authors thank Martin Miles for statistical and language consultation.

Author Contributions: V.M. and I.E. conceived, designed and performed the experiments and analyzed the data; V.M. wrote the paper.

Conflicts of Interest: The authors declare no conflict of interest.

References

1. Sailor, D.J.; Lu, L. A top-down methodology for developing diurnal and seasonal anthropogenic heating profiles for urban areas. *Atmos. Environ.* **2004**, *38*, 2737–2748. [CrossRef]
2. Kalnay, E.; Cai, M. Impact of urbanization and land-use change on climate. *Nature* **2003**, *423*, 528–531. [CrossRef] [PubMed]
3. Zhao, L.; Lee, X.; Smith, R.B.; Oleson, K. Strong contributions of local background climate to urban heat islands. *Nature* **2014**, *511*, 214–219. [CrossRef] [PubMed]
4. Zipper, S.C.; Schatz, J.; Singh, A.; Kucharik, C.J.; Townsend, P.A.; Loheide, S.P. Urban heat island impacts on plant phenology: Intra-urban variability and response to land cover. *Environ. Res. Lett.* **2016**, *11*, 054023. [CrossRef]
5. Knapp, S.; Kuhn, I.; Stolle, J.; Klotz, S. Changes in the functional composition of a Central European urban flora over three centuries. Perspectives in Plant Ecology. *Evol. Syst.* **2010**, *12*, 235–244.
6. Alcoforado, M.J.; Andrade, H. Global warming and the urban heat island. In *Urban Ecology*; Springer US: New York, NY, USA, 2008; pp. 249–262.
7. Wienert, U.; Kuttler, W. The dependence of the urban heat island intensity on latitude—A statistical approach. *Meteorol. Z.* **2005**, *14*, 677–686. [CrossRef] [PubMed]
8. Hinkel, K.M.; Nelson, F.E. Anthropogenic heat island at Barrow. Alaska, during winter: 2001–2005. *J. Geophys. Res.* **2007**, *112*, D06118. [CrossRef]
9. Konstantinov, P.I.; Grishchenko, M.Y.; Varentsov, M.I. Mapping Urban Heat Islands of Arctic Cities Using Combined Data on Field Measurements and Satellite Images Based on the Example of the City of Apatity (Murmansk Oblast). Izvestiya. *Atmos. Ocean. Phys.* **2015**, *51*, 992–998. [CrossRef]
10. Streletskiy, D.A.; Shiklomanov, N.; Grebenets, V. Changes of foundation bearing capacity due to climate warming in northwest Siberia. *Earth Cryosphere* **2012**, *16*, 22–32.
11. Shiklomanov, N.I.; Streletskiy, D.A.; Swales, T.W.; Kokorev, V.A. Climate change and stability of urban infrastructure in Russian permafrost regions: Prognostic assessment based on GCM climate projections. *Geogr. Rev.* **2016**, *107*, 1–18. [CrossRef]
12. Zhang, X.; Friedl, M.A.; Schaaf, C.B.; Strahler, A.H. Climate controls on vegetation phenological patterns in northern mid- and high latitudes inferred from MODIS data. *Glob. Chang. Biol.* **2004**, *10*, 1133–1145. [CrossRef]
13. Miles, V.; Esau, I. Spatial heterogeneity of greening and browning between and within bioclimatic zones in northern West Siberia. *Environ. Res. Let.* **2016**, *11*, 115002. [CrossRef]
14. Taha, H. Urban climates and heat islands: Albedo, evapotranspiration and anthropogenic heat. *Energy Build* **1997**, *25*, 99–103. [CrossRef]
15. McCarthy, M.P.; Best, M.J.; Betts, R.A. Climate change in cities due to global warming and urban effects. *Geophys. Res. Lett.* **2010**, *37*, L09705. [CrossRef]
16. Imhoff, M.L.; Zhang, P.; Wolfe, R.E.; Bounoua, L. Remote sensing of the urban heat island effect across biomes in the continental USA. *Remote Sens. Environ.* **2010**, *114*, 504–513. [CrossRef]
17. Li, Y.; Zhao, M.; Motesharrei, S.; Mu, Q.; Kalnay, E.; Li, S. Local cooling and warming effects of forests based on satellite observations. *Nat. Commun.* **2015**, *6*, 6603. [CrossRef] [PubMed]
18. Zhou, B.; Rybski, D.; Kropp, J.P. On the statistics of urban heat island intensity. *Geophys. Res. Lett.* **2013**, *40*, 5486–5491. [CrossRef]
19. Oke, T.R. City size and the urban heat island. *Atmos. Environ.* **1973**, *7*, 769–779. [CrossRef]

20. Christen, A.; Vogt, R. Energy and radiation balance of a central European city. *Int. J. Climatol.* **2004**, *24*, 1395–1421. [CrossRef]
21. Voogt, J.A. Urban Heat Island: Hotter Cities, 2004. ActionBioscience.org. Available online: http://www.actionbioscience.org/environment/voogt.html (accessed on 28 August 2017).
22. Huang, W.; Li, J.; Guo, Q.; Mansaray, L.R.; Li, X.; Huang, J. A Satellite-Derived Climatological Analysis of Urban Heat Island over Shanghai during 2000–2013. *Remote Sens.* **2017**, *9*, 641. [CrossRef]
23. Peng, S.; Piao, S.; Ciais, P.; Friedlingstein, P.; Ottle, C.; Bréon, F.-M.; Nan, H.; Zhou, L.; Myneni, R.B. Surface Urban Heat Island Across 419 Global Big Cities. *Environ. Sci. Technol.* **2012**, *46*, 696–703. [CrossRef] [PubMed]
24. Hu, L.; Brunsell, N.A. A new perspective to assess the urban heat island through remotely sensed atmospheric profiles. *Remote Sens. Environ.* **2015**, *158*, 393–406. [CrossRef]
25. Bosilovich, M.G. A comparison of MODIS land surface temperature with in situ observations. *Geophys. Res. Lett.* **2006**, *233*, L20112. [CrossRef]
26. Wang, W.; Liang, S.; Meyers, T. Validating MODIS land surface temperature products using long-term nighttime ground measurements. *Remote Sens. Environ.* **2008**, *112*, 623–635. [CrossRef]
27. Clinton, N.; Gong, P. MODIS detected surface urban heat islands and sinks: Global locations and controls. *Remote Sens. Environ.* **2013**, *134*, 294–304. [CrossRef]
28. Davy, R.; Esau, I. Differences in the efficacy of climate forcings explained by variations in atmospheric boundary layer depth. *Nat. Commun.* **2016**, *7*, 11690. [CrossRef] [PubMed]
29. Davy, R.; Esau, I.; Chernokulsky, A.; Outten, S.; Zilitinkevich, S. Diurnal asymmetry to the observed global warming. *Int. J. Climatol.* **2017**, *37*, 79–93. [CrossRef]
30. Kottek, M.; Grieser, J.; Beck, C.; Rudolf, B.; Rubel, F. World Map of the Köppen-Geiger climate classification updated. *Meteorol. Z.* **2006**, *15*, 259–263. [CrossRef]
31. Li, Z.-L.; Tang, B.-H.; Wu, H.; Ren, H.; Yan, G.; Wan, Z.; Trigo, I.F.; Sobrino, J.A. Satellite-derived land surface temperature: Current status and perspectives. *Remote Sens. Environ.* **2013**, *131*, 14–37. [CrossRef]
32. Hachem, S.; Duguay, C.R.; Allard, M. Comparison of MODIS-derived land surface temperatures with ground surface and air temperature measurements in continuous permafrost terrain. *Cryosphere* **2012**, *6*, 51–69. [CrossRef]
33. Schwarz, N.; Lautenbach, S.; Seppelt, R. Exploring indicators for quantifying surface urban heat islands of European cities with MODIS land surface temperatures. *Remote Sens. Environ.* **2011**, *115*, 3175–3186. [CrossRef]
34. Tan, M.; Quantifying, X.L. The effects of settlement size on urban heat islands in fairly uniform geographic areas. *Habitat Int.* **2015**, *49*, 100e106. [CrossRef]
35. Wang, C.; Myint, S.W.; Wang, Z.; Song, J. Spatio-temporal modeling of the urban heat island in the Phoenix metropolitan area: Land use change implications. *Remote Sens.* **2016**, *8*, 185. [CrossRef]
36. Shannon, C. A mathematical theory of communication. *Bell Syst. Tech. J.* **1948**, *27*, 379–423. [CrossRef]
37. Esau, I.; Miles, V.; Davy, R.; Miles, M.; Kurchatova, A. Trends in normalized difference vegetation index (NDVI) associated with urban development in northern West Siberia. *Atmos. Chem. Phys.* **2016**, *16*, 9563–9577. [CrossRef]
38. Esau, I.; Miles, V. Warmer urban climates for development of green spaces in northern Siberian cities. *Geogr. Environ. Sustain.* **2016**, *9*, 48–62. [CrossRef]
39. Brunsell, N.A.; Mechem, D.B.; Anderson, M.C. Surface heterogeneity impacts on boundary layer dynamics via energy balance partitioning. *Atmos. Chem. Phys.* **2011**, *11*, 3403–3416. [CrossRef]
40. Li, D.; Bou-Zeid, E. Synergistic Interactions between Urban Heat Islands and Heat Waves: The Impact in Cities Is Larger than the Sum of Its Parts. *J. Appl. Meteorol. Climatol.* **2013**, *52*, 2051–2064. [CrossRef]
41. Li, D.; Katul, G.G.; Zilitinkevich, S.S. Revisiting the Turbulent Prandtl Number in an Idealized Atmospheric Surface Layer. *J. Atmos. Sci.* **2015**, *72*, 2394–2410. [CrossRef]
42. Oleson, K. Contrasts between Urban and Rural Climate in CCSM4 CMIP5 Climate Change Scenarios. *J. Clim.* **2012**, *25*, 1390–1412. [CrossRef]
43. Beck, P.; Goetz, S. Satellite observations of high northern latitude vegetation productivity changes between 1982 and 2008: Ecological variability and regional differences. *Environ. Res. Lett.* **2011**, *6*, 045501. [CrossRef]
44. Esau, I. Amplification of turbulent exchange over wide Arctic leads: Large-eddy simulation study. *J. Geophys. Res.* **2007**, *112*, D08109. [CrossRef]

45. Van Heerwaarden, C.C.; Mellado, J.P.; Lozar, A.D. Scaling Laws for the Heterogeneously Heated Free Convective Boundary Layer. *J. Atmos. Sci.* **2014**, *71*, 3975–4000. [CrossRef]
46. Oke, T.R. The energetic basis of the urban heat island. *Q. J. R. Meteorol. Soc.* **1982**, *108*, 1–24. [CrossRef]
47. Memon, R.A.; Dennis, L.; Liu, C. A review on the generation, determination and mitigation of Urban Heat Island. *J. Environ. Sci.* **2008**, *20*, 120–128.
48. Zhou, D.; Zhao, S.; Zhang, L.; Sun, G.; Liu, Y. The footprint of urban heat island effect in China. *Sci. Rep.* **2015**, *5*, 11160. [CrossRef] [PubMed]
49. Steeneveld, G.J.; Koopmans, S.; Heusinkveld, B.G.; van Hove, L.W. A.; Holtslag, A.A.M. Quantifying urban heat island effects and human comfort for cities of variable size and urban morphology in the Netherlands. *J. Geophys. Res.* **2011**, *116*, D20129. [CrossRef]
50. Stroppiana, D.; Antoninetti, M.; Brivio, P.A. Seasonality of MODIS LST over Southern Italy and correlation with land cover, topography and solar radiation. *Eur. J. Remote Sens.* **2014**, *47*, 133–152. [CrossRef]
51. Cheval, S.; Dumitrescu, A. The summer surface urban heat island of Bucharest (Romania) retrieved from MODIS images. *Theor. Appl. Climatol.* **2015**, *121*, 631–640. [CrossRef]
52. Tomlinson, C.J.; Chapman, L.; Thornes, J.E.; Baker, C.J. Derivation of Birmingham's summer surface urban heat island from MODIS satellite images. *Int. J. Climatol.* **2012**, *32*, 214–224. [CrossRef]



© 2017 by the authors. Licensee MDPI, Basel, Switzerland. This article is an open access article distributed under the terms and conditions of the Creative Commons Attribution (CC BY) license (http://creativecommons.org/licenses/by/4.0/).